Petroleum Science 19 (2022) 220–233

Contents lists available at ScienceDirect

Petroleum Science

journal homepage: www.keaipublishing.com/en/journals/petroleum-science

Original Paper

Effects of creep characteristics of natural gas hydrate-bearing sediments on wellbore stability

Yang Li, Yuan-Fang Cheng, Chuan-Liang Yan*, Zhi-Yuan Wang, Li-Fang Song

School of Petroleum Engineering, China University of Petroleum (East China), 66 West Changjiang Road, Huangdao District, Qingdao 266000, China

ARTICLE INFO

Article history:
Received 14 October 2020
Accepted 28 October 2021
Available online 30 October 2021

Edited by Yan-Hua Sun

Keywords:
Natural gas hydrates
Wellbore stability
Creep
Plastic yield

ABSTRACT

Natural gas hydrate (NGH) reservoirs consist of the types of sediments with weak cementation, low strength, high plasticity, and high creep. Based on the kinetics and thermodynamic characteristics of NGH decomposition, herein a heat-fluid-solid coupling model was established for studying the wellbore stability in an NGH-bearing formation to analyze the effects of the creep characteristics of NGH-bearing sediments during long-term drilling. The results demonstrated that the creep characteristics of sediments resulted in larger plastic yield range, thus aggravating the plastic strain accumulation around the wellbore. Furthermore, the creep characteristics of NGH-bearing sediments could enhance the effects induced by the difference in horizontal *in situ* stress, as a result, the plastic strain in the formation around the wellbore increased nonlinearly with increasing difference in *in situ* stress. The lower the pore pressure, the greater the stress concentration effects and the higher the plastic strain at the wellbore. Moreover, the lower the initial NGH saturation, the greater the initial plastic strain and yield range and the higher the equivalent creep stress. The plastic strain at the wellbore increased nonlinearly with decreasing initial saturation.

1. Introduction

With rapid socioeconomic advancement, the development of conventional fossil energy cannot meet the increasing demand for energy at the global scale, thus more attention is being paid to unconventional oil and gas resources, including natural gas hydrates (NGHs). At high pressures and low temperatures, a large amount of natural gas gets trapped within a crystal structure of water to form NGHs (Englezos, 1993; Chong et al., 2016; Han et al., 2020). Studies have shown that NGHs are regarded as high-potential candidates for future energy due to their abundant geological reserves and high carbon content (Yan et al., 2018; Song et al., 2019). Therefore, extensive research efforts have been devoted to the exploration and development of NGHs at the global scale (Moridis et al., 2009; Song et al., 2014).

NGHs are buried at shallow depths; therefore, it is necessary to construct flow channels for natural gas between the reservoirs and the surface through drilling. Moreover, the wellbore stability during drilling of NGH reservoir is the key to determining whether NGHs can be produced or not (Sun et al., 2018; Li et al., 2020b). Compared to conventional formations, NGH reservoirs belong to the type of sediments with weak cementation, low strength, high plasticity, and creep characteristics (Ding et al., 2020; Hyodo et al., 2009; Rutqvist et al., 2012). During drilling, the NGHs around wellbores can get decomposed, which further reduces the formation strength due to engineering disturbances, resulting in a high risk of wellbore instability (Sun et al., 2018; Li et al., 2020a). Owing to the uniqueness and complexity of wellbore stability in NGH reservoirs, experts and scholars worldwide have conducted many studies.

Based on numerical calculations, Rutqvist et al. (2012) proposed that increasing drilling fluid column pressure could effectively maintain the stability of the well wall. Sun et al. (2018) stated that the decomposition of hydrate in the formation could be inhibited by controlling the drilling fluid salinity, which could maintain the wellbore stability. Furthermore, Wei et al. (2019) revealed that in order to protect hydrate-bearing strata, an increase in the density of drilling fluids should be avoided; nonetheless, cooling of the drilling fluids and shortening of the drilling time could be an effective method for protecting hydrate formations. Therefore, better effects can be obtained by focusing upon cooling of the drilling fluid and

* Corresponding author.
E-mail address: yanchuanliang@163.com (C.-L. Yan).

https://doi.org/10.1016/j.petsci.2021.10.026

Nomenclature

a, b	Experimental parameters of the NGHs
c	Soil cohesion (MPa)
c_r, c_h	Specific heat capacities of rock and NGHs (J/(kg·°C)
c_w, c_g	Specific heat capacities of water and gas (J/(kg·°C)
$c_{(S_h=0)}$	Cohesion of hydrate-free sand (MPa)
$c(S_h)$	Cohesion of hydrate sand (MPa)
$\bar{c}$	Comprehensive specific heat capacity (J/(kg·°C)
$\boldsymbol{D}$	Stiffness matrix
E	Activation energy (J/mol)
$E_{(S_h=0)}$	Elastic model of hydrate-free sand (MPa)
$E_{(S_h)}$	Elastic model of hydrate sand (MPa)
f	Body force vector
F	Plastic yield stress (MPa)
h	Heat flux per unit area of the body flowing into the body
h_a	Heat absorption rate during NGH decomposition (10^6 J/(m^3·s))
h_r	Heat of reactions during NGH decomposition (53 kJ/mol)
k	Effective permeability (mD)
k_0	Initial permeability of the porous media (mD)
k_d^0	Constant of decomposition rate of NGHs (36000 mol/(MPa·m^2·s))
l_1, l_2, l_3	Material parameters
l_4, l_5, l_6, l_7	Material parameters of creep property
$-\dot{m}_H$	Decomposition rate of the NGHs (kg/(m^2•s))
$\dot{m}_w$	Generation rates of natural gas and generation rates of water (kg/(m^3·s))
M_h	Molar mass of 1 mol of NGHs (mol/kg)
M_g, M_w	Molecular mass of methane and molecular mass of water (mol/kg)
$\boldsymbol{n}$	S-outside normal direction
p	Equivalent pressure stress (MPa)
P_{ep}	NGH phase-equilibrium pressure at temperature T (MPa)
P_p	Pore pressure (Pa)
q	von Mises equivalent stress (MPa)
Q	Plastic flow potential
r	Heat supplied internally into the body per unit volume
R	Universal gas constant (8.314 J/(mol/K))
S_a	Surface area under surface traction
S_h	Hydrate saturation
S_g, S_w	Gas saturation and water saturation
t	Time (s)
t_s	Surface traction vector
T	Temperature (K)
ΔT	Temperature difference
$\dot{U}$	Rate of increase in soil energy over time
$\boldsymbol{v}_{fp}$	Percolation velocity
w	Effective stress coefficient ($w = 1$)
α	Thermal expansion coefficient
$\delta\boldsymbol{T}$	An arbitrary variational field satisfying the essential boundary conditions
$\delta\boldsymbol{\varepsilon}$	Virtual strain rate matrix
$\delta\boldsymbol{v}$	Virtual velocity vector
ε_c	Creep strain (%)
ε_c'	Creep rate over any time increment (%·s^{-1})
ε_v	Volume strain
$\Delta\varepsilon_c$	Creep strain over any time increment
θ	Internal friction angle (°)
$\boldsymbol{\lambda}$	Heat transfer coefficient matrix
$\bar{\lambda}$	Comprehensive coefficient of thermal conductivity (W/(m·°C)
λ_w, λ_g	Coefficients of thermal conductivity of water and gas (W/(m·°C)
λ_r, λ_h	Coefficients of thermal conductivity of rock and NGHs (W/(m·°C)
ρ	Density of material (g/cm^3)
ρ_f	Pore fluid density (g/cm^3)
σ_3	Confining pressure (MPa)
$\boldsymbol{\sigma}$	Total stress matrix
$\bar{\sigma}^{cr}$	Equivalent creep stress (MPa)
$\boldsymbol{\sigma}'$	Effective stress
τ	Shear stress (MPa)
φ	Solid medium porosity
φ_0	Initial porosity of hydrate-free sand
ψ	Dilatancy angle (°)

reduction in the drilling time. Based on the evolution characteristics of the plastic zones around a wellbore in an NGH-bearing formation, Li et al. (2020b) revealed that the range of the plastic zones in the formation was determined based on the NGH decomposition range. Moreover, the reason why plastic zones with a secondary stress concentration in an undecomposed NGH formation constantly developed away from the wellbore was explained. In these studies, researchers have mainly focused on the influences of NGH decomposition behavior on the wellbore stability, which is indeed an extremely important factor impacting wellbore walls in NGH-bearing formations. However, the effects of the creep characteristics of NGH-bearing formations have been totally ignored.

Noteworthy, as an NGH-bearing formation is developed as the objective layer, horizontal drilling needs to be conducted to improve productivity, which prolongs the drilling period (Feng et al., 2017a). In this case, creep is an important factor that cannot be neglected. Importantly, creep refers to the phenomenon whereby the deformation of a solid increases over time under a constant load (Hyodo et al., 2009). The creep characteristics of a formation result in the shrinkage of wellbores and sticking of drill pipe, and a formation with high plasticity leads to the increase in the risk of collapse of wellbore walls, even causing wellbore failure. Furthermore, Yan et al. (2018) pointed out that the plastic and creep deformations around wellbores in NGH-bearing sediments were used to jointly determine the final wellbore shrinkage and were affected by the *in situ* stress and strength of the NGH-bearing formation. However, in this model, the phenomenon of NGH decomposition during drilling was ignored; moreover, the effects of the creep characteristics of sediments on the mechanical responses of the formation around wellbores were not analyzed. Therefore, the effects of the creep characteristics of NGH-bearing sediments on the wellbore stability have rarely been explored till date. In this study, a heat-fluid-solid coupled numerical model was built to determine via calculations the influences of the creep characteristics of NGH-bearing sediments on the wellbore stability during the drilling of NGH reservoirs. The reasons for the generation of such effects were systematically analyzed from a mechanical perspective. Based on this, herein the effects of hydrate decomposition, drilling time, ratio of the initial *in situ* stress, formation pore pressure, and initial NGH saturation on the wellbore stability were

analyzed. The research results could provide reference for long-term drilling schemes for NGH-bearing formations.

2. Mathematical model

Noteworthy, the drilling process in hydrate formations is accompanied by changes in formation pore pressure, stress, and temperature. When the formation temperature and pressure around the wellbore do not meet the phase equilibrium conditions of the hydrate, the hydrate tends to decompose. As a result, the seepage, mechanics, and heat transfer properties of the formation change and react to the distribution of pore pressure, stress, and temperature field. The essence is a four-field coupling process shown in Fig. 1.

2.1. Basic governing equations

The basic governing equation of hydrate formation seepage field can be determined by using the mass balance Eq. (1) (Zhu et al., 2015; SIMULIA, 2016; Gao et al., 2019):

$$\frac{\mathrm{d}}{\mathrm{d}t}\left(\int_V \rho_\mathrm{f}\varphi \mathrm{d}V\right) = -\int_S \rho_\mathrm{f}\boldsymbol{n}\cdot\boldsymbol{v}_\mathrm{fp}\mathrm{d}S \tag{1}$$

The solid mechanics of hydrate formation follows the principle of virtual work, and its control equation can be represented as Eq. (2) (Li et al., 2019; Feng et al., 2017b):

$$\int_V \boldsymbol{\sigma} : \delta\boldsymbol{\varepsilon}\mathrm{d}V = \int_{S_\mathrm{a}} \boldsymbol{t}_\mathrm{s}\delta\boldsymbol{v}\mathrm{d}V + \int_V \boldsymbol{f}\delta\boldsymbol{v}\mathrm{d}V \tag{2}$$

According to the law of conservation of energy, the temperature field control equation of the hydrate formation can be represented as follows (Li et al., 2020a):

$$\int_V \left(\rho\dot{U}\delta\boldsymbol{T}\right)\mathrm{d}V + \int_V \left(\frac{\partial\delta\boldsymbol{T}}{\partial x}\cdot\lambda\cdot\frac{\partial\boldsymbol{T}}{\partial x}\right)\mathrm{d}V = \int_V \left(\delta\boldsymbol{T}r\right)\mathrm{d}V + \int_{sq}\left(\delta\boldsymbol{T}h\right)\mathrm{d}S \tag{3}$$

Noteworthy, only under certain temperature and pressure conditions, methane molecules and water molecules can together form stable crystalline compounds. Thus, the phase equilibrium equation of methane hydrate can be denoted in terms of Eq. (4) (Kamath, 1998).

$$P_\mathrm{eq} = \mathrm{e}^{a-\frac{b}{T}} \tag{4}$$

When the ambient temperature and pressure conditions do not satisfy the phase equilibrium equation, the hydrate decomposition rate is represented as Eq. (5) (Kim et al., 1987; Sun and Mohanty, 2006; Zheng et al., 2018):

$$-\dot{m}_\mathrm{H} = M_\mathrm{h}k_\mathrm{d}^0\mathrm{e}^{-\frac{E}{RT}}\sqrt{\frac{\varphi^3\left(S_\mathrm{g}+S_\mathrm{w}\right)}{2k}}\left(P_\mathrm{eq}-P_\mathrm{p}\right) \tag{5}$$

The generation rate of methane gas and liquid water can be represented in terms of Eqs. (6) and (7), respectively (Alavi and Ripmeester, 2010; Jin et al., 2016).

$$\dot{m}_\mathrm{g} = -\dot{m}_\mathrm{h}\frac{M_\mathrm{g}}{M_\mathrm{h}} \tag{6}$$

$$\dot{m}_\mathrm{w} = 6(-\dot{m}_\mathrm{h})\frac{M_\mathrm{w}}{M_\mathrm{h}} \tag{7}$$

Further, the formation and decomposition of methane hydrate are accompanied by the latent heat of phase change, and the equation used for calculation can be represented as Eq. (8) (Hu et al., 2017).

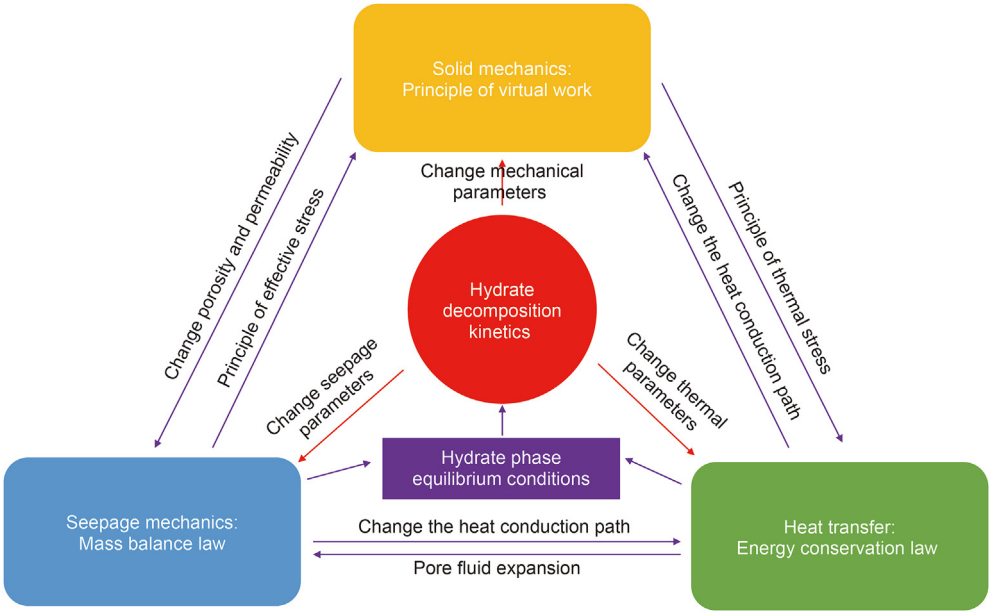

Fig. 1. Schematic illustration of coupled model.

$$h_a = h_r \frac{\dot{m}_h}{M_h} \tag{8}$$

2.2. Mechanics model of hydrate sediment

2.2.1. Plasticity law

The linear Drucker–Prager yield criterion is used to describe the plastic behavior of hydrate sediments. The plastic yield surface can be described by Eq. (9) (Li et al., 2020a):

$$F = q - p\tan\beta - d = 0 \tag{9}$$

When the Drucker–Prager parameters associated with the Mohr–Coulomb criterion are used, the parameters β and d can be shown in Eqs. (10) and (11) (SIMULIA, 2016).

$$\sin\theta = \frac{\tan\beta\sqrt{3(9-\tan^2\psi)}}{9-\tan\beta\tan\psi} \tag{10}$$

$$c\cos\theta = \frac{\sqrt{3(9-\tan^2\psi)}}{9-\tan\beta\tan\psi} d \tag{11}$$

When the associated flow rules are used, the mathematical equation can be represented as Eq. (12):

$$Q = q - p\tan\psi \tag{12}$$

When considering the creep characteristics of sediments, the equivalent creep stress can be represented in terms of Eq. (13) (Yan et al., 2019):

$$\overline{\sigma}^{cr} = \frac{q - p\tan\beta}{1-(1/3)\tan\beta} \tag{13}$$

2.2.2. Influence of temperature field and pore pressure field on stress distribution

When considering the effect of temperature changes on the stress field distribution, the thermal stress can be represented in terms of Eq. (14).

$$\boldsymbol{\sigma} = \boldsymbol{D}\cdot\left(\boldsymbol{\varepsilon} - \alpha\Delta T[1 \quad 1 \quad 1 \quad 0 \quad 0 \quad 0]^T\right) \tag{14}$$

Further, when the effect of changes in pore pressure on the stress field distribution is considered, according to the effective stress principle, the actual force of the formation framework is shown as Eq. (15) (Gao et al., 2019; Huang et al., 2019).

$$\sigma' = \sigma - wp_p \tag{15}$$

2.3. Parameter equation of thermophysical properties of hydrate sediments

2.3.1. Porous media equation of hydrate sediments

The porosity and permeability of the formation constitute a decisive factor affecting the pore pressure conduction and pore fluid migration. Hydrate saturation and stress state of the formation have a strong influence on them. The formation framework rigidity is much greater than pore filling; therefore, it is assumed that the deformation of formation is caused by the compression of pores. The effective porosity of hydrate formation can be represented in terms of Eq. (16) (Yan et al., 2018).

$$\varphi = \frac{1}{1+\varepsilon_v}(\varphi_0(1-S_h)+\varepsilon_v) \tag{16}$$

The effective permeability under different hydrate saturation and stress state of formation can be represented in terms of Eq. (17) (Yan et al., 2018).

$$k = k_0\left[\frac{\varphi}{\varphi_0}\right]^5 \times \left[\frac{1-\varphi_0}{1-\varphi}\right]^2 \tag{17}$$

2.3.2. Thermal parameter equation of hydrate sediments

In the actual formation, the change of hydrate saturation leads to the change in the solid phase composition of the formation, and then affects the thermal conductivity. The thermal conductivity and specific heat capacity of hydrate formations at different hydrate saturations are represented in terms of Eqs. (18) and (19) (Li et al., 2020b, 2021).

$$\bar{\lambda} = \varphi(\lambda_w S_w + \lambda_g S_g) + (1-\varphi_0)\lambda_r + (\varphi_0-\varphi)\lambda_h \tag{18}$$

$$\bar{c} = \varphi(c_w S_w + c_g S_g) + (1-\varphi_0)c_r + (\varphi_0-\varphi)c_h \tag{19}$$

2.3.3. Mechanical parameter equation of hydrate sediments

In hydrate formations, the decomposition of hydrate leads to the sharp decrease in the rigidity and strength of the sediments. Thus, hydrate saturation is an important factor affecting mechanical properties. The research results show that the improved Mohr–Coulomb criterion can describe the strength performance of sediments as shown in Eq. (20) (Sun et al., 2018; Yoneda et al., 2015).

$$\tau = c(S_h) + \sigma_3\tan\theta = c_{(S_h=0)} + \frac{1-\sin\theta}{2\cos\theta} l_1 \cdot (100S_h)^{l_2} \tag{20}$$

Furthermore, a linear model can be used to characterize the variation of Young's modulus of hydrate sediments with hydrate saturation, as shown in Eq. (21).

$$E(S_h) = E_{(S_h=0)} + l_3 \cdot S_h \tag{21}$$

2.3.4. Creep equation of hydrate sediments

Miyazaki et al. (2011) conducted low-temperature triaxial creep tests on NGH samples at saturation of 0 and 48%, respectively. The results demonstrated that the NGH samples revealed obvious characteristics of creep attenuation in the low-stress state; in contrast, they exhibited accelerating creep characteristics in the high-stress state. In the drilling process of NGH-bearing formations, an excessive stress concentration can directly lead to the collapse of wellbore walls, thus the density of the drilling fluid is generally controlled to ensure the wellbore stability. Therefore, while analyzing the wellbore stability in NGH-bearing formations, in this study, the influences of accelerating creep on the wellbore stability were ignored. The creep attenuation in the experimental data was processed, and the results illustrated that the creep attenuation of the NGH samples meets the characteristics of a logarithmic function, as shown in Eq. (22).

$$\varepsilon_c = l_4 \cdot \lg(t) \tag{22}$$

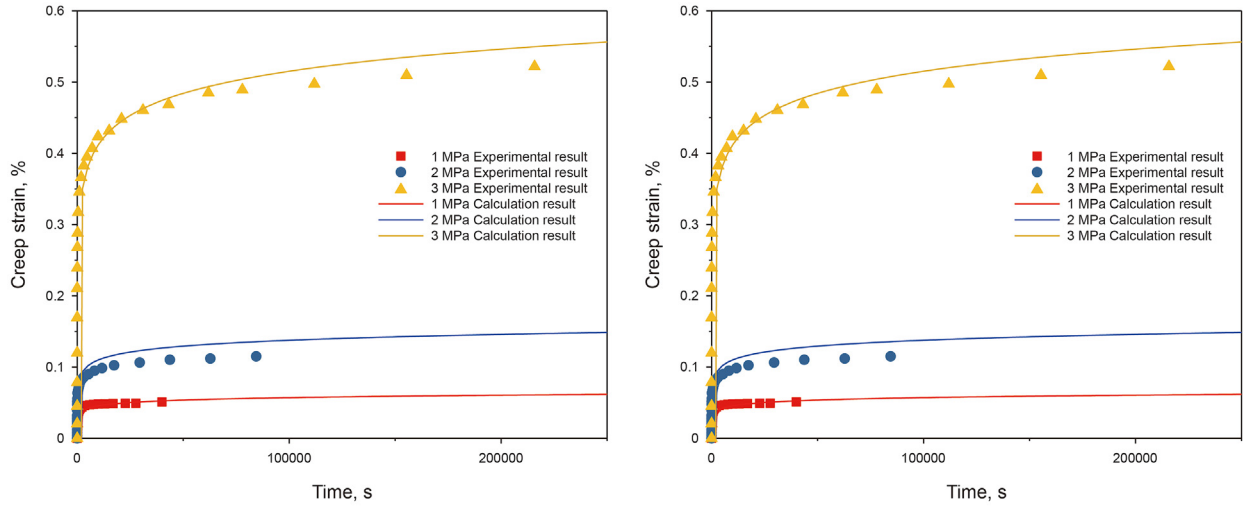

(a) Curve from the creep test at a saturation of 0% **(b)** Curve from the creep test at a saturation of 45.5%

Fig. 2. Curves from the triaxial creep tests on the NGH samples (Miyazaki et al., 2011).

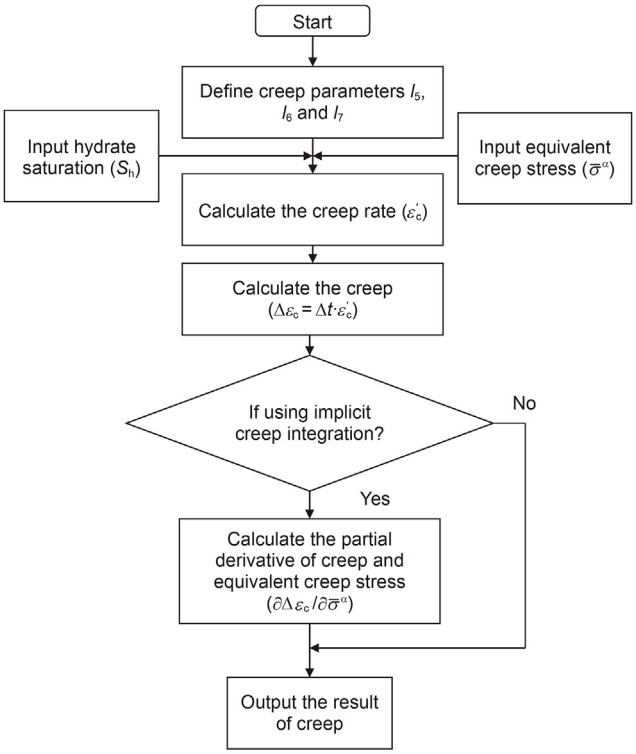

Fig. 3. Flow chart.

Noteworthy, saturation of only 0 and 45.5% were included in the experimental data. For this reason, assuming that the creep parameters of NGHs changed linearly with saturation, a creep model for the NGH samples with saturation was obtained and represented in terms of Eq. (23). It is evident from the fitting results shown in Fig. 2 that the logarithmic model attains a good fitting effect in regard to the creep characteristics of the NGHs.

$$\varepsilon_c = (l_5 \cdot S_h + l_6) \cdot \exp(l_7 \bar{\sigma}^{cr}) \cdot \lg(t) \tag{23}$$

where $l_5 = 0.0134$, $l_6 = 0.0038$ and $l_7 = 1.1$.

3. Introduction of the numerical model

The ABAQUS software was used to establish and calculate the numerical model. In this model, the USDFLD and HETVAL user subroutine were used to achieve the process of decomposition of NGHs, the details of these two user subroutines were provided by Li et al. (2020b). The CREEP user subroutine was applied to calculate the creep behavior of the NGH-bearing sediments.

3.1. CREEP user subroutine

The CREEP user subroutine is a secondary developed subprogram in ABAQUS software, which is used for the simulation of the creep characteristics of solid materials and can be combined with the USDFLD user subroutine to achieve the objective of controlling the parameters of the creep properties through field variables. Fig. 3 exhibits the specific implementation method. First, creep parameters l_5, l_6, and l_7 required for the calculations are defined, and then the distribution of the NGH saturation and equivalent creep stress $\bar{\sigma}^{cr}$ over this time increment are obtained. Moreover, the creep rate ε_c' and creep ε_c in the current state are calculated. Noteworthy, if the explicit integration method is applied, creep calculation results are directly obtained as output. In contrast, if implicit integration method is adopted, the partial derivative $\partial\Delta\varepsilon_c/\partial\bar{\sigma}^{cr}$ of the creep strain to the equivalent creep stress is further calculated, and the calculation results are subsequently provided as output.

According to Eq. (23), the creep strain rate over any time increment can be expressed as:

$$\varepsilon_c' = (l_5 \cdot S_h + l_6) \cdot e^{l_7 \bar{\sigma}^{cr}} \Big/ (t \cdot \ln(10)) \tag{24}$$

The partial derivative of the creep strain to the equivalent creep stress over any time increment, which is expressed as:

$$\frac{\partial\Delta\varepsilon_c}{\partial\bar{\sigma}^{cr}} = \frac{l_7 \Delta t}{(t \cdot \ln(10))} (l_5 \cdot S_h + l_6) \cdot e^{l_7 \bar{\sigma}^{cr}} \tag{25}$$

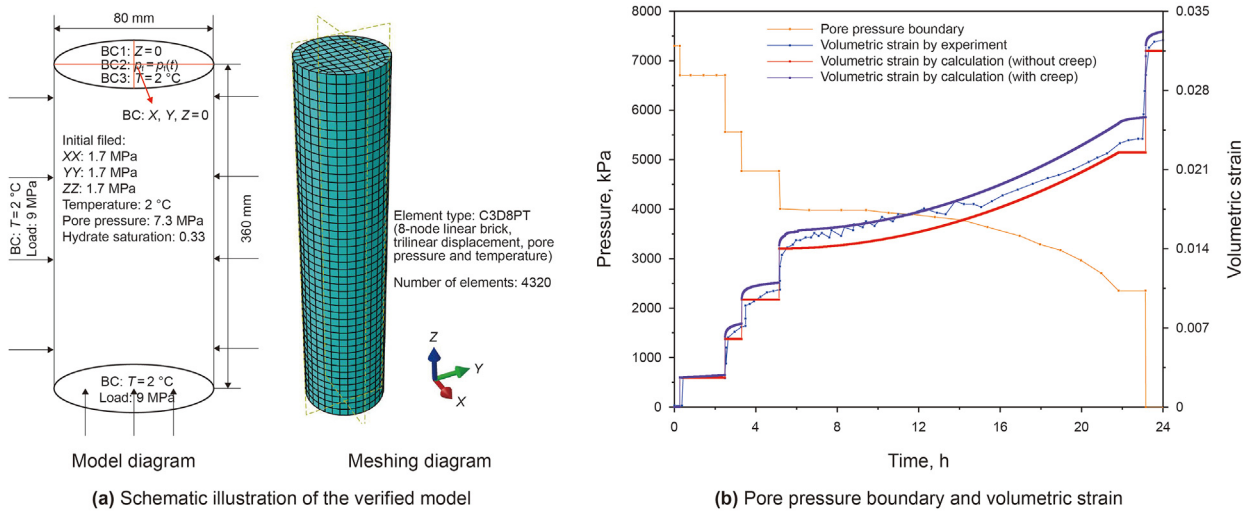

Fig. 4. Comparative analysis of verified model and calculated results (Gupta et al., 2017).

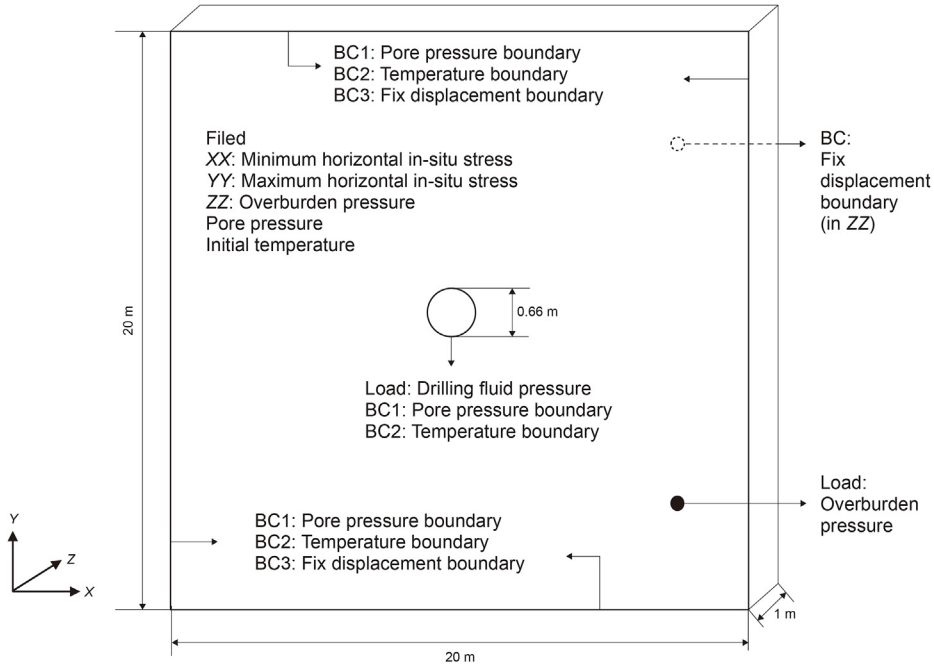

Fig. 5. Schematic illustration of the geometric model.

3.2. Model verification

In order to ensure the successful call of user subroutines, a model for the verification was established for carrying out comparative analysis with the experimental results provided by Gupta et al. (2017). Fig. 4a displays the model size, boundary conditions, and element types. The simulation process includes the following two analysis steps: The first step involves the application of initial variables and boundary conditions, and the second step includes the simulation of the pressure reduction process.

The detailed modeling process of the verification model is described in the literature study by Li et al. (2020b). Fig. 4b shows the curve of the pore pressure boundary and a curve exhibiting the comparison between the calculated results and experimental results. The results reveal that when the creep characteristics of the NGH samples are not considered, the calculated results are smaller than the measured results, with a maximum error of 13.2%. In contrast, when the creep characteristics of the NGH samples are considered, the calculated results are slightly larger than the measured values, and the maximum error is 11%. The fact that the calculated results are larger than the measured results can be explained as follows: Although the basic thermodynamic parameters of the model used for verification are the experimental results reported in previous literature study, the creep parameters are the experimental results obtained by Miyazaki et al. (2011) rather than the results obtained by using the same experimental system. Moreover, the creep parameters include only the experimental results obtained at saturation of 0 and 45.5%, and the intermediate data correspond to linear assumptions, which may be the reason for the occurrence of these errors. The main objective of this study is to

Table 1
Load, boundary, and field in numerical model.

Position	Load/Boundary/Field	Step 1	Step 2
Suf 1/Suf 2	Boundary: $YY = 0$	Active	Active
Suf 3/Suf 4	Boundary: $XX = 0$	Active	Active
Suf 6	Boundary: $ZZ = 0$	Active	Active
Suf 5	Load: Overburden pressure	Active	Active
Suf 1/Suf 2/Suf 3/Suf 4	Boundary: Pore pressure	Active	Active
Suf 1/Suf 2/Suf 3/Suf 4	Boundary: Temperature	Active	Active
Suf 7	Boundary: $XX = YY = ZZ = 0$	Active	Inactive
Suf 7	Boundary: Pore pressure		Active
Suf 7	Boundary: Temperature		Active
Suf 7	Load: Drilling fluid pressure		Active
All	Field: Minimum horizontal *in situ* stress (*XX*)	Active	Active
All	Field: Maximum horizontal *in situ* stress (*YY*)	Active	Active
All	Field: Overburden pressure (*ZZ*)	Active	Active
All	Field: Pore pressure	Active	Active
All	Field: Initial temperature	Active	Active
All	Field: Initial hydrate saturation	Active	Active

Note: Suf 1 is the upper surface, Suf 2 is the lower surface, Suf 3 is the left surface, Suf 4 is the right surface, Suf 5 is the front surface, Suf 6 is the back surface, Suf 7 is the wellbore, and All denotes the entire model.

Table 2
Parameters used for numerical model.

Parameter	Value
Overburden pressure	21.8 MPa
Horizontal *in situ* stress (Maximum)	20.45 MPa
Horizontal *in situ* stress (Minimum)	19.7 MPa
Pore pressure	17 MPa
In situ temperature	15.15 °C
Thermal conductivity (water)	0.6 W/(m·°C)
Thermal conductivity (methane)	0.00335 W/(m·°C)
Thermal conductivity (hydrates)	0.4 W/(m·°C)
Thermal conductivity (formation)	1.5 W/(m·°C)
Specific heat (water)	4.2 kJ/(kg·°C)
Specific heat (methane)	2.093 kJ/(kg·°C)
Specific heat (hydrates)	2.1 kJ/(kg·°C)
Specific heat (formation)	1.6 kJ/(kg·°C)
Density (water)	1.0 g/cm^3
Density (hydrates)	0.91 g/cm^3
Density (formation)	2.2 g/cm^3
Initial permeability	1 mD
Initial porosity	0.5
Initial hydrate saturation	0.5
Effective stress coefficient	1.0
Elastic model of hydrate-free sand	35.414 MPa
Parameter l_3	517.57
Cohesion of hydrate-free sand	0.1 MPa
Parameter l_1	0.0011
Parameter l_2	1.91
Internal friction angle	30°
Dilatancy angle	0°
Creep parameter l_5	0.0134
Creep parameter l_6	0.0038
Creep parameter l_7	1.1
Parameter a	39
Parameter b	8533
Drilling fluid pressure	16 MPa
Drilling fluid temperature	30 °C

analyze the mechanism of the influence of creep properties on the mechanical behaviors of wellbores, and some numerical errors are acceptable. Therefore, it is reasonable to use the established model to evaluate the effects of the creep characteristics on the drilling of NGH reservoirs.

3.3. The model for wellbore stability

The three-dimensional (3D) numerical model, with 20 m length, 20 m width, 1 m thickness, and 0.33 m radius of wellbore, was built as shown in Fig. 5. The load, boundary conditions, and initial filed in each step are listed in Table 1. The element type is C3D8PT and the total number of elements of the model is 43200.

In order to prevent the invasion of drilling fluid into the formation, underbalanced drilling was selected. To consider the influence of NGH decomposition on the wellbore walls, a high-temperature drilling fluid was adopted to ensure that the temperature and pressure of the formation around the wellbore were separated from the range of the NGH phase equilibrium. Table 2 lists the parameters required for the model calculations (Wei et al., 2019; Yoneda et al., 2015; Miyazaki et al., 2010).

4. Effects of the creep characteristics of NGH-bearing sediments on the mechanical behaviors of wellbores

In order to analyze the influence of creep characteristics of NGH-bearing sediments on the mechanical behavior of the wellbore wall, a contrast model without consideration of the creep characteristics of the sediments but under the same remaining conditions was established. Fig. 6 shows the temperature, pore pressure, and NGH saturation distribution after 24 h of wellbore drilling as well as cloud pictures of the distribution of plastic strain of the two models (calculated results based on distance of 1.2 m away from the wellbore were selected). Owing to the influence of the drilling fluid on the formation pore pressure and temperature, after 24 h of wellbore drilling, the NGHs in the formation within 0.35 m from the wellbore were found to be completely decomposed. Moreover, the NGH decomposition front reached 0.47 m. NGH decomposition resulted in the reduction in the elasticity and strength of the formation, which caused changes of the stress distribution in the formation, promoted the development of plastic zones in the formation, and affected the wellbore stability (Li et al., 2020b). Irrespective of the consideration of the creep characteristics of NGH-bearing sediments, the formation with completely decomposed NGHs surrounding the wellbore enters the plastic state. Although plastic zones are distributed in the same range, the distribution characteristics of the plastic strain reveal that the creep characteristics of NGH-bearing sediments significantly affect the development of plastic zones around the wellbore. First, when the creep characteristics of NGH-bearing sediments are not taken into consideration, the distribution of plastic zones around the wellbore is obviously correlated with the difference in the horizontal *in situ* stress. In other words, plastic zones mainly develop in the direction of the minimum horizontal *in situ* stress, and the entire plastic zone is oval in shape. Moreover, the ratio of the maximum plastic strain

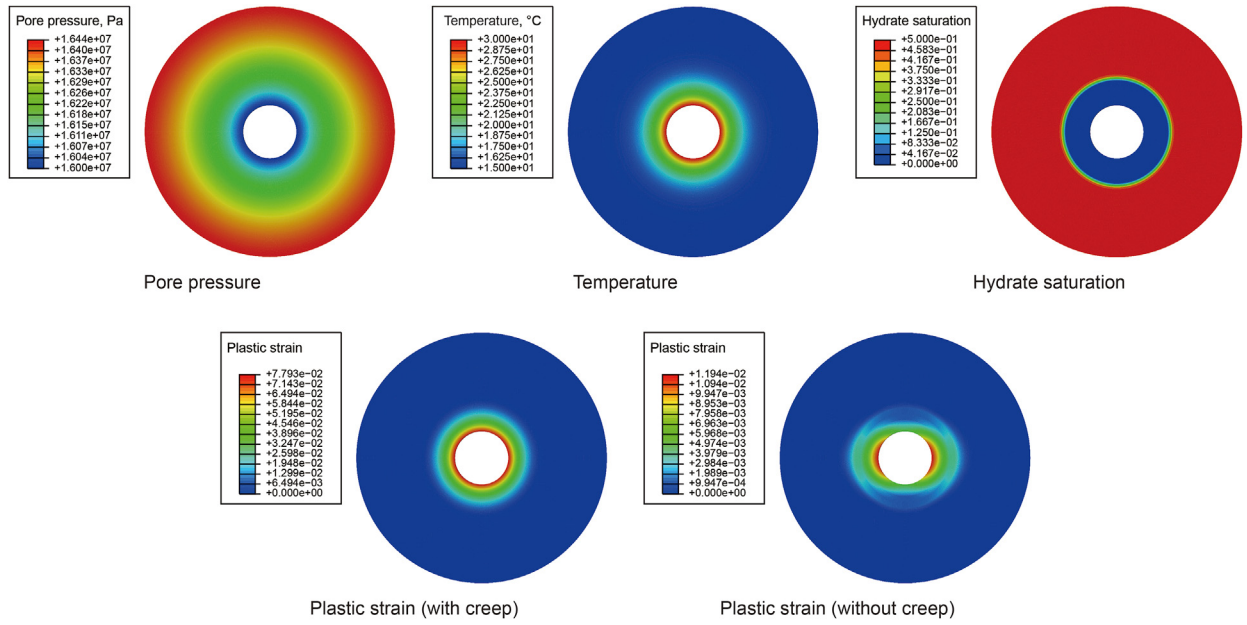

Fig. 6. Distributions of the temperature, pressure, NGH saturation, and plastic strain around the wellbore.

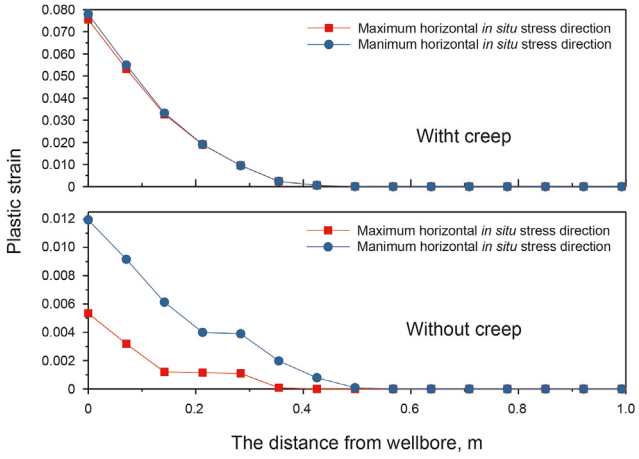

Fig. 7. Distributions of the plastic strain in the formation in the directions of the maximum and minimum horizontal *in situ* stresses.

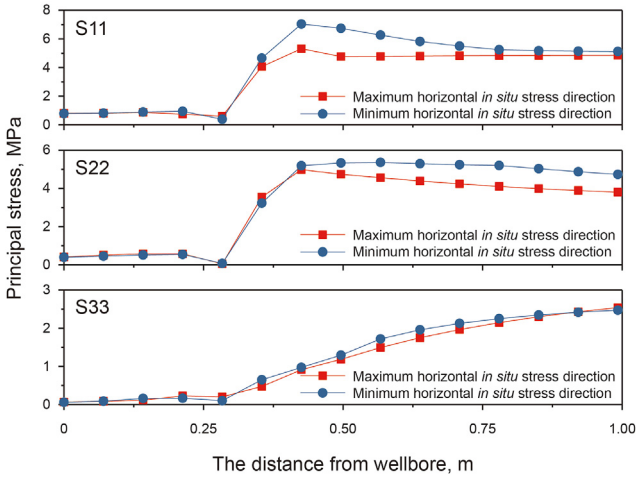

Fig. 8. Stress distribution in the NGH-bearing formation without considering creep characteristics.

to the minimum strain at the wellbore wall is 2.23. In contrast, when the creep characteristics of NGH-bearing sediments are considered, clearly, the plastic zone develops more uniformly and the entire plastic zone is approximately circular. The ratio of the maximum plastic strain to the minimum strain at the wall is only 1.032, as shown in Fig. 7. The diameter of the circle is close to the major axis of elliptical plastic zone calculated without considering the creep characteristics. Second, it is observed that the creep characteristics of NGH-bearing sediments lead to the significant increase in the plastic strain in the plastic zones around the wellbore. Without considering the creep characteristics, the maximum plastic strain at the wellbore wall is 0.012; however, the plastic strain is 0.078 when considering the creep characteristics. Noteworthy, the latter is 6.5 times the former.

Figs. 8 and 9 show distributions of the principal stress in the formation in the directions of the maximum and minimum *in situ* stresses, respectively, around the wellbores in the two models after 24 h of wellbore drilling. Attributed to the plastic deformation of the formation near the wellbore and the reduction in elastic properties due to NGH decomposition, the stress on the wellbore wall and in the formation near the wellbore is no longer the maximum, and obvious secondary stress concentration occurs in the transition zone of the NGH saturation (Li et al., 2020b). In case the creep characteristics are not taken into consideration, the near-wellbore zone is affected by plastic deformation (0.0–0.3 m), and the principal stresses along the two directions coincide. However, the stress distribution of the formation in the secondary stress concentration area shows obvious directional difference. The maximum principal stress in the direction of the minimum horizontal *in situ* stress is higher than that in the direction of the maximum horizontal *in situ* stress. This indicates further enhancement in the directional difference in the distribution of the plastic zones around the wellbore with the further increase in the wellbore drilling time. Nonetheless, when the creep characteristics of NGHs are considered, completely different results are obtained. After 24 h of wellbore drilling, the principal stress in the formation

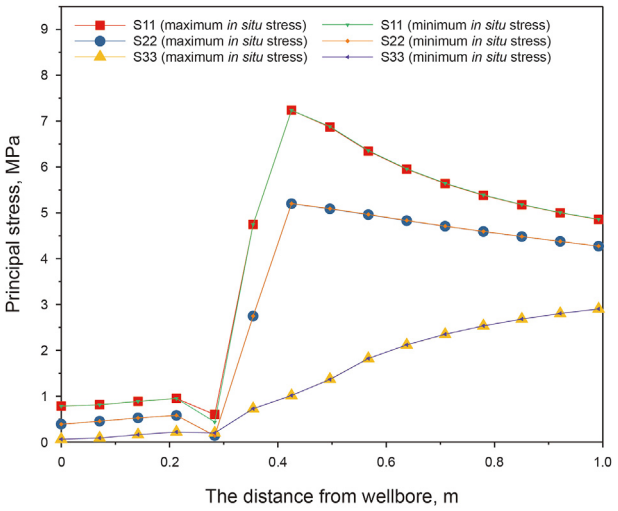

Fig. 9. Stress distribution in the NGH-bearing formation considering creep characteristics.

in the two directions almost overlaps. This indicates that the subsequent deformation of the wellbore is no longer controlled by the *in situ* stress and maintains a uniform and synchronous development thereafter. Comparative analysis of the results of the two models indicates that the principal stress distribution in secondary stress concentration area (with creep) is almost consistent with that in the direction of the minimum horizontal *in situ* stress (without creep). For example, the values of maximum principal stress in the minimum and maximum horizontal ground stress directions are 7.1 and 5.3 MPa at 0.4 m (without creep), respectively. When the creep characteristics are considered, the maximum principal stress in both directions at this location is 7.2 MPa. It indicates that the maximum principal stress in all directions of wellbore gradually approaches the stress distribution in the direction of the original maximum principal stress with the largest value. Fig. 10 shows the evolution of the plastic zones around the borehole, clearly indicating that the initial plastic zones around the wellbore are mainly concentrated in the direction of the minimum horizontal *in situ* stress. With the increase in the wellbore drilling time, the difference induced by the nonuniform *in situ* stress gradually decreases, and the range of the plastic zones enlarges with the increase in the NGH decomposition range.

Therefore, during the drilling of NGH-bearing formations, the initial plastic deformation occurs at the very moment when the formation is drilled in response to stress concentration. With the increase in drilling time, NGHs gradually decompose and the range of the plastic zones enlarges. The plastic zone undergoes gradual transitions into a circle shape from an ellipse. The range of the plastic zones in the formation around the wellbore is determined by using the NGH decomposition range. The creep characteristics

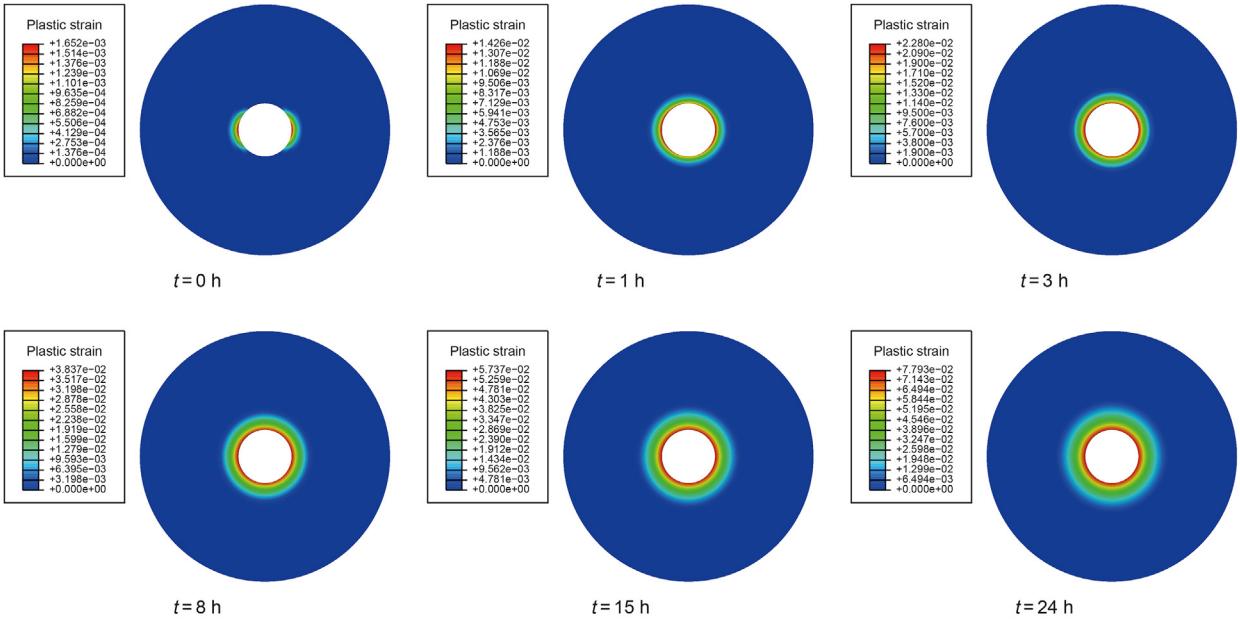

Fig. 10. Evolution of the plastic zones around the wellbore.

Table 3
Effective *in situ* stress.

Ratio of the effective horizontal *in situ* stress	Minimum horizontal effective *in situ* stress, MPa	Maximum horizontal effective *in situ* stress, MPa	Effective overburden pressure, MPa
1.00	3.45	3.45	4.80
1.05	3.29	3.45	4.80
1.10	3.14	3.45	4.80
1.15	3.00	3.45	4.80
1.20	2.88	3.45	4.80
1.25	2.76	3.45	4.80
1.28	2.70	3.45	4.80
1.30	2.65	3.45	4.80

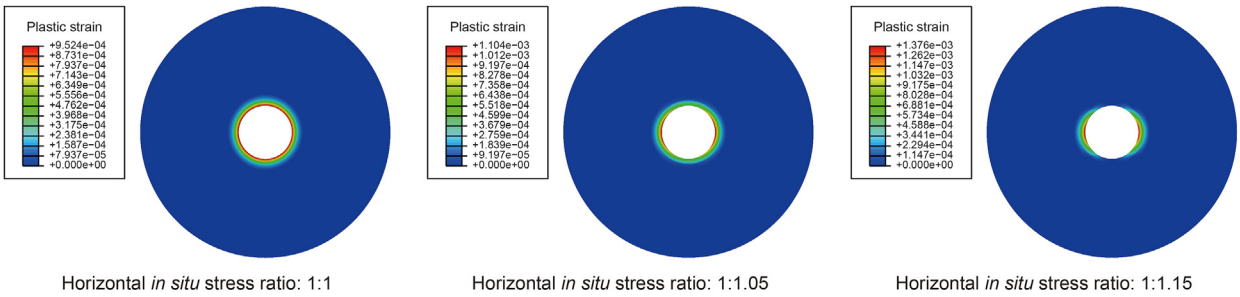

Fig. 11. Cloud picture of the initial plastic strain under various differences in the effective horizontal *in situ* stress.

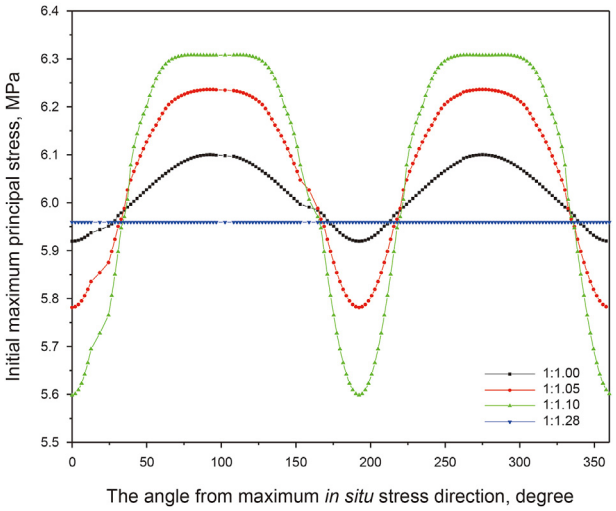

Fig. 12. Initial maximum principal stress distribution in the wellbore under various differences in the effective horizontal *in situ* stress.

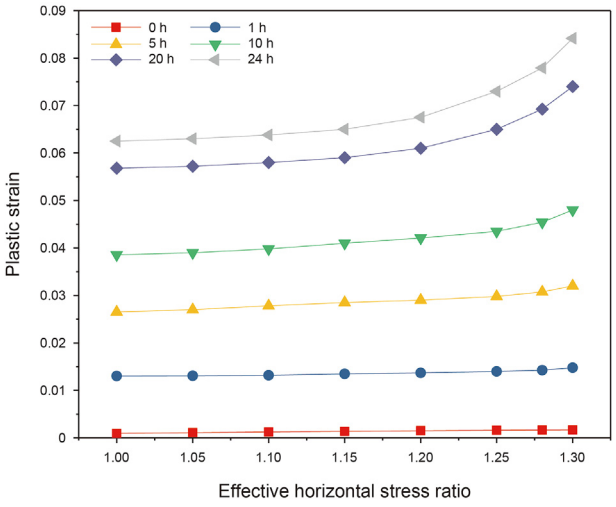

Fig. 13. Changes in the maximum plastic strain in the wellbore wall with the change in the ratio of the effective horizontal *in situ* stress.

result in the maximum principal stress in all directions of wellbore approaching the stress distribution of the direction of the original maximum principal stress with the largest value. This aggravates the development of the plastic strain caused by the stress state in the formation around the wellbore. Creep deformation also leads to the acceleration of the accumulative rate of wellbore plastic strain, thereby leading to high collapse risks.

5. Analysis of factors influencing wellbore stability in NGH reservoirs

5.1. Influences of the difference in the horizontal in situ stress on the wellbore stability

The compaction effect of the upper formation on the lower formation produces complex *in situ* stress field and heterogeneities in the formation. However, under the influence of tectonic movement, the *in situ* stress exhibits a difference in the horizontal direction, and different formations show different *in situ* stress differences due to their different tectonic movement histories. During the drilling process, a difference in the horizontal *in situ* stress could lead to a difference in the stress concentration around the wellbore in different directions. Moreover, an excessively large difference in the horizontal *in situ* stress is unfavorable for ensuring the wellbore stability. Thus, in this study, a model for the wellbore stability considering different ratios of the effective horizontal *in situ* stress ($\sigma_H : \sigma_h$) was established to analyze the effects of these ratios on the wellbore stability during the decomposition and creep process of NGH-bearing sediments. The maximum effective horizontal *in situ* stress is maintained constant, and the specific values are listed in Table 3.

Fig. 11 shows cloud pictures of the initial plastic strain under various differences in the effective horizontal *in situ* stress. The figure illustrates that when the wellbore is just drilled, the higher the ratio of the effective horizontal *in situ* stress, the higher the nonuniformity of the plastic zone distribution in the formation around the wellbore and the maximum the plastic strain of the wellbore. This result is attributed to the following reason: the moment at which the wellbore opens, the stability of the NGHs is maintained and the state of wellbore is determined only in terms of the stress state and strength of the formation. A larger difference in the horizontal *in situ* stress indicates a higher nonuniformity in the stress state around the wellbore, such that the shear stress in the formation around the wellbore increases. Fig. 12 shows the initial maximum principal stress distribution in the wellbore under various differences in the effective horizontal *in situ* stress (0° represents the maximum horizontal *in situ* stress direction). A larger difference in the horizontal *in situ* stress results in the increase in the initial maximum principal stress in the formation around the wellbore. The formation more easily enters the plastic state and produces a higher creep stress. With increasing wellbore drilling time, the creep characteristics of NGH-bearing sediments lead to the reduction in the difference in the direction of the stress distribution. The wellbore stress state makes it harder to maintain the wellbore stability. Therefore, with the increase in the wellbore

Table 4
Initial effective *in situ* stress.

Pore pressure, MPa	Minimum horizontal effective *in situ* stress, MPa	Maximum horizontal effective *in situ* stress, MPa	Effective overburden pressure, MPa
16	3.7	4.45	5.8
17	2.7	3.45	4.8
18	1.7	2.45	3.8

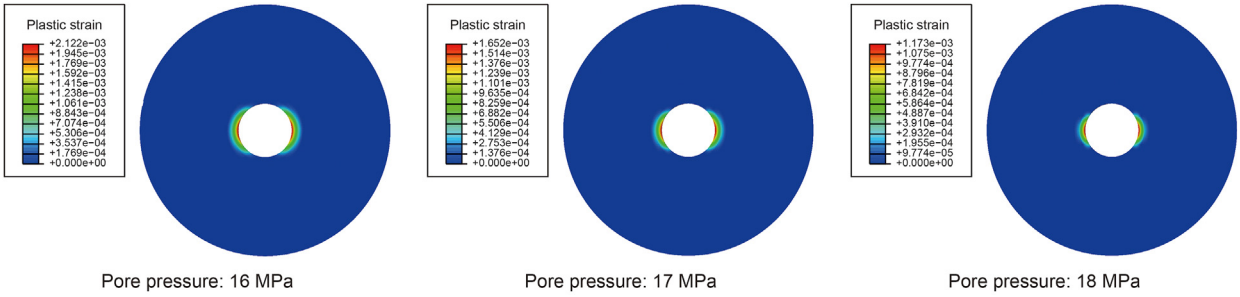

Fig. 14. Initial plastic strain under different formation pore pressures.

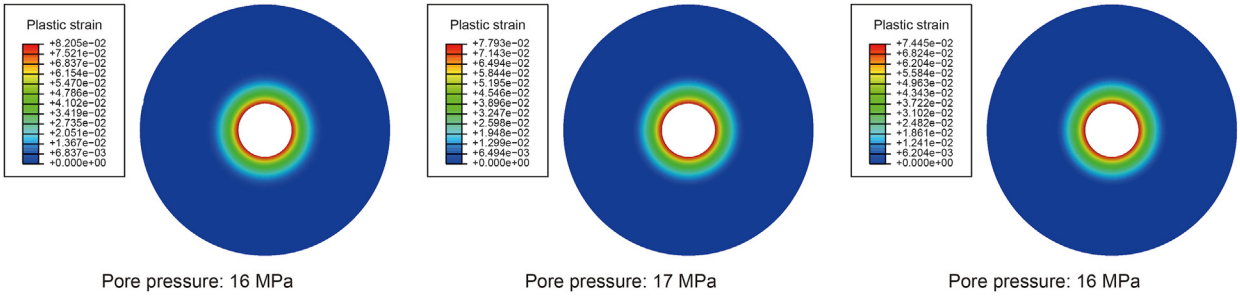

Fig. 15. Plastic strain after 24 h of drilling under different formation pore pressures.

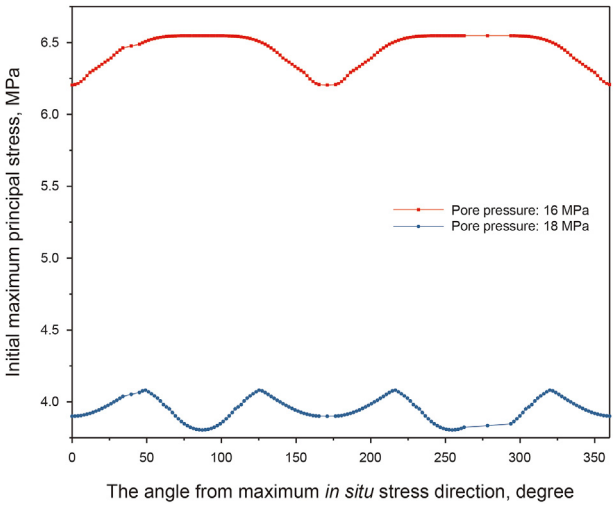

Fig. 16. Principal stress distribution in the wellbore at the initial moment.

drilling time, the influence of the ratio of the horizontal *in situ* stress on the wellbore plastic strain gets further enhanced, as shown in Fig. 13. After 1 h of wellbore drilling, the maximum plastic strain in the wellbore is 0.0131 when the ratio of the effective horizontal *in situ* stress is 1:1 (namely, a uniform *in situ* stress); however, with the change in the ratio to 1:1.3, the maximum plastic strain reaches 0.0148. The changes in the *in situ* stress result in the increase in the maximum plastic strain in the wellbore by 0.0017. After 24 h of wellbore drilling, the maximum plastic strain in the wellbore reaches 0.063 at a ratio of the effective horizontal *in situ* stress of 1:1, while it is 0.085 at a ratio of 1:1.3, showing that the maximum plastic strain increases by 0.022.

Therefore, larger difference in the horizontal *in situ* stress leads to the greater plastic deformation in the formation around the wellbore, which is more unfavorable for the wellbore stability. With the increase in the wellbore drilling time, the creep characteristics of NGH-bearing sediments further lead to the increase in the influences exerted by differences in the horizontal *in situ* stress and accelerate the accumulation of the plastic strain in the formation around the wellbore. Finally, it results in the nonlinear increase in plastic strain in the formation around the wellbore with the increase in ratio of the horizontal *in situ* stress. Therefore, larger difference in the horizontal *in situ* stress causes the higher risk of wellbore instability in NGH-bearing sediments. Moreover, with increasing wellbore drilling time, effects of the difference in the horizontal *in situ* stress on the wellbore stability further increase.

5.2. Effects of pore pressure on the wellbore stability

In deep-sea formations, the pore pressure comprises the pressure of the hydrostatic column of sea water from the water surface to the seabed mudline and the pressure of the hydrostatic column generated by the pore fluid in the formation. Noteworthy, the formation pore pressure is an important component of the initial effective stress distribution in the formation, and different

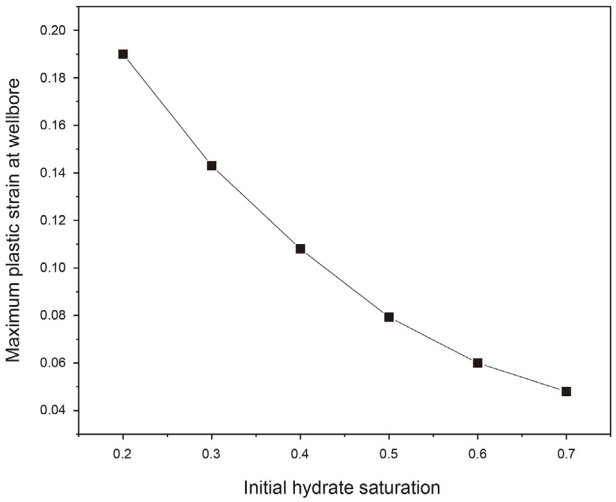

Fig. 17. Changes in the maximum plastic strain in the wellbore wall with the initial NGH saturation.

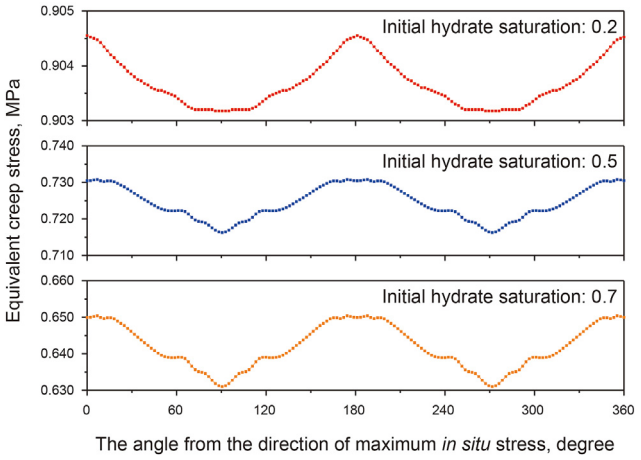

Fig. 19. Distribution of the equivalent creep stress in the wellbore wall after 24 h of wellbore drilling.

formation pore pressure alters the effective stress around the wellbore and eventually affects the mechanical behavior of wellbore walls. Moreover, in an NGH-bearing formation, the formation pore pressure is an important factor responsible for maintaining the NGH stability. Therefore, different formation pore pressures exert major effects on the wellbore stability of NGH-bearing formations. In this study, a mechanical analysis model of a wellbore under formation pore pressures of 16, 17, and 18 MPa was established to analyze the effects of the formation pore pressures on the wellbore stability. The values of initial effective stress of the formation are listed in Table 4.

With the continuous increase in the formation pore pressure, the initial plastic strain around the wellbore and the plastic strain in the formation after 24 h of drilling decrease, as shown in Figs. 14 and 15, respectively. At the initiation of the wellbore drilling, the formation pore pressure is 16 MPa, and the maximum plastic strain around the wellbore is 0.002122. However, with the increase in the formation pore pressure to 18 MPa, the maximum plastic strain becomes 0.001173. This happens due to the fact that the higher formation pore pressure produces lower effective *in situ* stress in the formation, which results in a smaller stress concentration effect. Fig. 16 illustrates the maximum principal stress distribution in the wellbore at the initial moment under formation pore pressures of 16 and 18 MPa, respectively. Evidently, a higher pore pressure leads to a lower maximum principal stress in the wellbore, such that the initial plastic strain in the wellbore decreases. Moreover, the stress state determines the creep stress, thus affecting the subsequent mechanical behavior of the wellbore. Finally, the plastic strain in the wellbore increases with decreasing formation pore pressure.

5.3. Impacts of the initial NGH saturation on the wellbore stability

The well logging data of an NGH-bearing formation indicate that the NGH saturation is nonuniform. The initial NGH saturation significantly affects the initial mechanical properties of the formation around the wellbore, which results in different stress distribution after wellbore drilling followed by a series of different deformation laws of wellbores. Therefore, exploration of the influences of the initial NGH saturation on the wellbore stability in NGH-bearing formations could provide an important guidance for selecting the location of a wellbore for subsequent drilling. Herein, a mechanical analysis model for the wellbore at initial NGH saturations of 0.3, 0.4, 0.5, 0.6, and 0.7 was built to analyze the effects of the initial NGH saturation on the mechanical responses during NGH decomposition, creep, and yield of NGH reservoirs.

Fig. 17 shows a curve of the variation in the maximum plastic strain in the wellbore with the initial NGH saturation after 24 h of wellbore drilling. Clearly, the maximum plastic strain in the wellbore nonlinearly increases with decreasing initial NGH saturation. When the initial NGH saturation in the reservoir is 0.7, the maximum plastic strain in the wellbore wall is 0.048, while it is 0.19 at a saturation of 0.2, which is 3.96 times the former value. This is attributed to the fact that the lower the initial NGH saturation, the lower the strength of NGH-bearing sediments, thus the range of the initial plastic yield zone around the wellbore at the beginning of drilling and the plastic yield value increase, as shown in Fig. 18. Further, when the initial saturation of the NGH reservoirs is 0.2, the

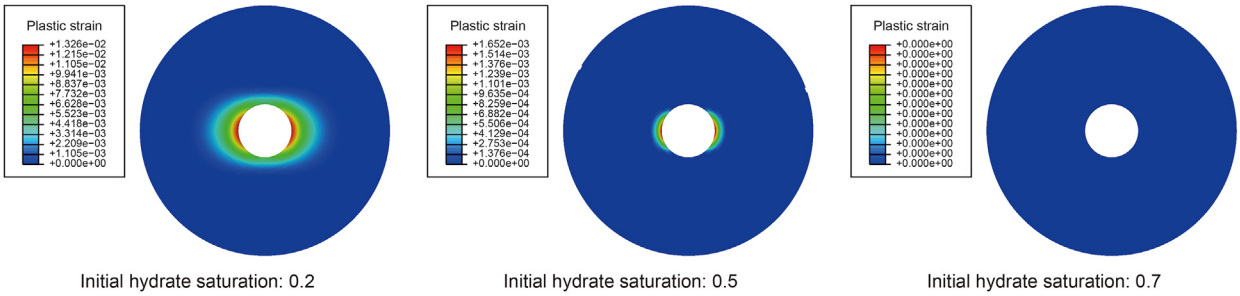

Fig. 18. Distribution of the initial plastic strain in the wellbore wall with the hydrate saturation.

stress concentration generated at the initial moment of drilling could lead to the plastic yield of the entire formation around the wellbore, and the maximum plastic strain reaches 0.01326. At an initial NGH saturation of 0.5, yield occurs only in part of the formation around the wellbore wall in the direction of the minimum horizontal *in situ* stress, and the maximum plastic strain is 0.001652. Moreover, at an initial NGH saturation of 0.7, plastic yield does not occur at all around the wellbore. Thus, importantly, the different initial saturations of the NGH reservoirs could change the stress distribution in the formation around the wellbore. Fig. 19 demonstrates that after 24 h of wellbore drilling, the equivalent creep stress around the wellbore decreases gradually with increasing initial NGH saturation. For example, at an initial saturation of 0.7, the equivalent creep stress is 0.65 MPa, which reaches 0.9 MPa at an initial saturation of 0.2. This clearly indicates that under the same wellbore drilling time, the lower value of initial NGH saturation leads to the higher creep strain. Furthermore, under the same drilling time, the equivalent creep stress is the highest in the direction of the maximum horizontal *in situ* stress; nonetheless, it is the lowest in the direction of the minimum horizontal *in situ* stress. Consequently, the difference in plastic deformation caused by the offset of the *in situ* stress difference could be mitigated.

The initial saturation of the NGH-bearing formation significantly influences the subsequent mechanical response after wellbore drilling. The lower value of initial saturation results in the lower strength of the sediments and greater initial plastic strain and yield range around the wellbore. Furthermore, the equivalent creep stress increases under the same drilling time. This finally leads to the nonlinear increase in the plastic strain in the wellbore with decreasing initial saturation. Therefore, during the actual drilling process, drilling a formation with a high NGH saturation is conducive to maintaining the wellbore stability without considering the natural gas invasion.

6. Conclusions

(1) In the drilling process of natural gas hydrate (NGH)-bearing formations, initial plastic deformation occurs due to stress concentration at initial moment. However, with increasing drilling time, NGHs gradually decompose and the plastic zone enlarges and gradually changes into a circular shaped zone. The range of the plastic yield is determined in terms of the NGH decomposition range.

(2) The creep characteristics of NGH sediments lead to the elimination of the difference in the direction of stress distribution. Moreover, creep characteristics result in the increase in the range of plastic yield zone and accelerate the wellbore plastic strain accumulation. Owing to the influence of the stress concentration and creep characteristics of NGH-bearing sediments, the plastic deformation of the formation around the wellbore constantly increases, leading to the continuous increase in the risk of collapse with increasing drilling time.

(3) Larger difference in the horizontal *in situ* stress leads to the greater plastic deformation that could be produced in the formation around the wellbore. With increasing wellbore drilling time, the creep characteristics of NGH-bearing sediments enhance the influences exerted by the differences in the horizontal *in situ* stress and further accelerate the accumulation of the plastic strain in the formation around the wellbore. Moreover, this finally results in the nonlinear increase in plastic strain in the formation around the wellbore with increasing ratio of the horizontal *in situ* stress.

(4) The lower pore pressure of the formation generates the higher effective *in situ* stress in the formation and the maximum principal stress in the wellbore. This produces a higher creep stress while determining plastic development, finally showing the increase in the plastic strain in the wellbore with decreasing formation pore pressure.

(5) Initial saturation of the NGH-bearing formation affects the mechanical responses of the formation around the wellbore. The lower value of initial saturation leads to the lower strength of the sediments and the greater initial plastic strain and yield range around the wellbore. Moreover, under the same drilling time, the equivalent creep stress in the wellbore increases. Finally, this is manifested as the nonlinear increase in the plastic strain in the wellbore with decreasing initial saturation. Consequently, the results of this study indicate that in the actual drilling process, without considering natural gas invasion, drilling through a formation with a high NGH saturation is beneficial to maintaining the wellbore stability.

Acknowledgement

This work is financially supported by the National Natural Science Foundation of China (51974353, 51991362), Natural Science Foundation of Shandong Province (ZR2019ZD14), CNPC's Major Science and Technology Projects (ZD2019-184-003).

References

Alavi, S., Ripmeester, J.A., 2010. Nonequilibrium adiabatic molecular dynamics simulations of methane clathrate hydrate decomposition. J. Chem. Phys. 132 (14), 144703. https://doi.org/10.1063/1.3382341.

Chong, Z.R., Yang, S.H.B.Y., Babu, P., Linga, P., Li, X.S., 2016. Review of natural gas hydrates as an energy resource: prospects and challenges. Appl. Energy 162, 1633–1652. https://doi.org/10.1016/j.apenergy.2014.12.061.

Ding, J., Cheng, Y., Deng, F., Yan, C., Sun, H., Li, Q., Song, B., 2020. Experimental study on dynamic acoustic characteristics of natural gas hydrate sediments at different depths. Int. J. Hydrogen Energy 45 (51), 26877–26889. https://doi.org/10.1016/j.ijhydene.2020.06.295.

Englezos, P., 1993. Clathrate hydrates. Ind. Eng. Chem. Res. 32 (7), 1251–1274.

Feng, J., Wang, Y., Li, X., 2017a. Entropy generation analysis of hydrate dissociation by depressurization with horizontal well in different scales of hydrate reservoirs. Energy 125, 62–71. https://doi.org/10.1016/j.energy.2017.02.104.

Feng, Y., Li, X., Gray, K., 2017b. Development of a 3D numerical model for quantifying fluid-driven interface debonding of an injector well. Int. J. Greenh. Gas. Con. 62, 76–90. https://doi.org/10.1016/j.ijggc.2017.04.008.

Gao, Q., Cheng, Y., Han, S., Yan, C., Jiang, L., 2019. Numerical modeling of hydraulic fracture propagation behaviors influenced by pre-existing injection and production wells. J. Petrol. Sci. Eng. 172, 976–987. https://doi.org/10.1016/j.petrol.2018.09.005.

Gupta, S., Deusner, C., Haeckel, M., Helmig, R., Wohlmuth, B., 2017. Testing a thermo-chemo-hydro-geomechanical model for gas hydrate-bearing sediments using triaxial compression laboratory experiments. G-cubed 18 (9), 3419–3437. https://doi.org/10.1002/2017GC006901.

Han, S., Gao, Q., Cheng, Y., Yan, C., Han, Z., Shi, X., 2020. Experimental study on brittle response of shale to cryogenic fluid nitrogen treatment. J. Petrol. Sci. Eng. 194, 107463. https://doi.org/10.1016/j.petrol.2020.107463.

Hu, Y., Lee, B.R., Sum, A.K., 2017. Insight into increased stability of methane hydrates at high pressure from phase equilibrium data and molecular structure. Fluid Phase Equil. 450, 24–29. https://doi.org/10.1016/j.fluid.2017.07.003.

Huang, N., Liu, R., Jiang, Y., Cheng, Y., Li, B., 2019. Shear-flow coupling characteristics of a three-dimensional discrete fracture network-fault model considering stress-induced aperture variations. J. Hydrol. 571, 416–424. https://doi.org/10.1016/j.jhydrol.2019.01.068.

Hyodo, M., Nakata, Y., Yoshimoto, N., et al., 2009. Bonding strength by methane hydrate formed among sand particles. In: Aip Conference. American Institute of Physics, pp. 79–82. https://doi.org/10.1063/1.3180049.

Jin, G., Xu, T., Xin, X., Wei, M., Liu, C., 2016. Numerical evaluation of the methane production from unconfined gas hydrate-bearing sediment by thermal stimulation and depressurization in Shenhu area, South China Sea. J. Nat. Gas Sci. Eng. 33, 497–508. https://doi.org/10.1016/j.jngse.2016.05.047.

Kamath, V.A., 1998. A perspective on gas production from hydrates. In: JNOC's Methane Hydrate Intl Symposium.

Kim, H.C., Bishnoi, P.R., Heidemann, R.A., Rizvi, S.S.H., 1987. Kinetics of methane hydrate decomposition. Chem. Eng. Sci. 42 (7), 1645–1653. https://doi.org/10.1016/0009-2509(87)80169-0.

Li, X., Mothar, E.C.S., Gray, K.E., 2019. Modeling progressive breakouts in deviated wellbores. J. Petrol. Sci. Eng. 175, 905–918. https://doi.org/10.1016/j.petrol.2019.01.007.

Li, Y., Cheng, Y., Yan, C., Song, L., Liu, H., Tian, W., Ren, X., 2020b. Mechanical study on the wellbore stability of horizontal wells in natural gas hydrate reservoirs. J. Nat. Gas Sci. Eng. 19, 103359. https://doi.org/10.1016/j.jngse.2020.103359.

Li, Y., Cheng, Y., Yan, C., Song, L., Zhou, X., Niu, C., 2020a. Influence of drilling fluid temperature on borehole shrinkage during drilling operation in cold regions. J. Petrol. Sci. Eng. 190, 107050. https://doi.org/10.1016/j.petrol.2020.107050.

Li, Y., Cheng, Y., Yan, C., Wang, Z., Zhang, Q., Zhou, P., 2021. Stratum settlement during depressurization of horizontal wells in gas hydrate reservoirs. Energ. Fuel. 35 (18), 14692–14708. https://doi.org/10.1021/acs.energyfuels.1c02249.

Miyazaki, K., Sakamoto, Y., Aoki, K., Tenma, N., 2011. Creep property of artificial methane-hydrate-bearing rock. In: 12th ISRM Congress. International Society for Rock Mechanics and Rock Engineering.

Miyazaki, K., Yamaguchi, T., Sakamoto, Y., Tenma, N., Ogata, Y., Aoki, K., 2010. Effect of confining pressure on mechanical properties of sediment containing synthetic methane hydrate. J MMIJ 126 (7), 408–417. https://doi.org/10.2473/journalofmmij.126.408.

Moridis, G.J., Collett, T.B.R., Kurihara, M., Reagan, M.T., Koh, C., Sloan, E.D., 2009. Toward production from gas hydrates: current status assessment of resources, and simulation-based evaluation of technology and potential. SPE Reservoir Eval. Eng. 12 (5), 745–771. https://doi.org/10.2118/114163-PA.

Rutqvist, J., Moridis, G.J., Grover, T., Silpngarmlert, S., Collett, T.S., Holdich, S.A., 2012. Coupled multiphase fluid flow and wellbore stability analysis associated with gas production from oceanic hydrate-bearing sediments. J. Petrol. Sci. Eng. 92, 65–81. https://doi.org/10.1016/j.petrol.2012.06.004.

SIMULIA, 2016. Abaqus Version 2016 Analysis User's Guide. Dassault Systemes, Providence, RI, USA.

Song, B., Cheng, Y., Yan, C., Lyu, Y., Wei, J., Ding, J., Li, Y., 2019. Seafloor subsidence response and submarine slope stability evaluation in response to hydrate dissociation. J. Nat. Gas Sci. Eng. 65, 197–211. https://doi.org/10.1016/j.jngse.2019.02.009.

Song, Y., Yang, L., Zhao, J., Liu, W., Yang, M., Li, Y., Liu, Y., Li, Q., 2014. The status of natural gas hydrate research in China: a review. Renew. Sustain. Energy Rev. 31, 778–791. https://doi.org/10.1016/j.rser.2013.12.025.

Sun, J., Ning, F., Lei, H., Gai, X., Sánchez, M., Lu, J., Li, Y., Liu, L., Liu, C., Wu, N., He, Y., Wu, M., 2018. Wellbore stability analysis during drilling through marine gas hydrate-bearing sediments in Shenhu area: a case study. J. Petrol. Sci. Eng. 170, 345–367. https://doi.org/10.1016/j.petrol.2018.06.032.

Sun, X., Mohanty, K.K., 2006. Kinetic simulation of methane hydrate formation and dissociation in porous media. Chem. Eng. Sci. 61 (11), 3476–3495. https://doi.org/10.1016/j.ces.2005.12.017.

Wei, J., Cheng, Y., Yan, C., Li, Q., Han, S., Ansari, U., 2019. Decomposition prevention through thermal sensitivity of hydrate formations around wellbore. Appl. Therm. Eng. 159, 113921. https://doi.org/10.1016/j.applthermaleng.2019.113921.

Yan, C., Li, Y., Yan, X., Cheng, Y., Han, Z., Tian, W., Ren, X., 2019. Wellbore shrinkage during drilling in methane hydrate reservoirs. Energy. Sci. Eng. 7 (3), 930–942. https://doi.org/10.1002/ese3.323.

Yan, C., Li, Y., Cheng, Y., Wang, W., Song, B., Deng, F., Feng, Y., 2018. Sand production evaluation during gas production from natural gas hydrates. J. Nat. Gas Sci. Eng. 57, 77–88. https://doi.org/10.1016/j.jngse.2018.07.006.

Yoneda, J., Masui, A., Konno, Y., Jin, Y., Egawa, K., Kida, M., Ito, T., Nagao, J., Tenma, N., 2015. Mechanical properties of hydrate-bearing turbidite reservoir in the first gas production test site of the Eastern Nankai Trough. Mar. Petrol. Geol. 66, 471–486. https://doi.org/10.1016/j.marpetgeo.2015.02.029.

Zheng, R., Li, S., Li, X., 2018. Sensitivity analysis of hydrate dissociation front conditioned to depressurization and wellbore heating. Mar. Petrol. Geol. 91, 631–638. https://doi.org/10.1016/j.marpetgeo.2018.01.01.

Zhu, H., Zhao, X., Guo, J., Jin, X., An, F., Wang, Y., Lai, X., 2015. Coupled flow-stress-damage simulation of deviated-wellbore fracturing in hard-rock. J. Nat. Gas Sci. Eng. 26, 711–724. https://doi.org/10.1016/j.jngse.2015.07.007.